Pure Appl. Chem., Vol. 81, No. 4, pp. 743–754, 2009.
doi:10.1351/PAC-CON-08-08-30

DNA nucleobase properties and photoreactivity: Modeling environmental effects*

Daniel Roca-Sanjuán[1], Gloria Olaso-González[1], Mercedes Rubio[1], Pedro B. Coto[1], Manuela Merchán[1], Nicolas Ferré[2], Valdemir Ludwig[3], and Luis Serrano-Andrés[1,‡]

[1]Institute of Molecular Science, University of València, Apartado de Correos 22085, ES-46071 València, Spain; [2]Universités d'Aix-Marseille I, II et III-CNRS, UMR 6264: Laboratoire Chimie Provence, Theoretical Chemistry, F-13397 Marseille Cedex 20, France; [3]Department of Physics, Universidade Federal do Mato Grosso do Sul CP 549, CEP 79070-900, Campo Grande, MS, Brazil

Abstract: The accurate ab initio quantum chemical (QM) method multiconfigurational second-order perturbation (CASSPT2)/complete active space self-consistent field (CASSCF) has been used in conjunction with molecular mechanics (MM) procedures to compute molecular properties and photoinduced reactivity of DNA/RNA nucleobases (NABs) in isolation and within a realistic environment, in which the double helix strand, the aqueous media, and the external counterions are included. It is illustrated that the use of an MM model is helpful both to account for short- and long-range effects of the system surrounding the QM molecular core and to provide the proper structural constraints that allow more accurate QM geometry determinations.

Keywords: quantum chemistry; solvent effects; photochemistry; DNA bases; QM/MM.

INTRODUCTION

In parallel to an intense period of experimental activity [1], the last few years have known a growing number of theoretical studies on the properties and photoreactivity of DNA components, in particular, the pyrimidine and purine nucleobases (NABs): uracil (U), thymine (T), cytosine (C), adenine (A), and guanine (G), as well as of close related derivatives and analogous, as monomers or dimers [2]. The use of modern quantum chemical (QM) methods for ground and excited states has enabled the accurate determination of properties such as ionization potentials (IPs) or electron affinities (EAs) (see, e.g., [3,4]), ground-state reactivity [5,6], and more recently excited-state reactivity, including excimer formation, photochemical dimerization, and NABs-photopharmacon adduct formation [7–9]. In particular for excited states, where the description of states degeneracy (in general conical intersections, CIs) is required, the multiconfigurational approaches have been the protagonists of the achievements, in particular the ab initio complete active space self-consistent field (CASSCF) and the multiconfigurational second-order perturbation (CASPT2) methods [10–13], and to a minor extent other multiconfigurational procedures such as the combined density functional theory/multireference configuration interac-

*Paper based on a presentation at the 19th International Conference on Physical Organic Chemistry (ICPOC-19), 13–18 July 2008, Santiago de Compostela, Spain. Other presentations are published in this issue, pp. 571–776.

‡Corresponding author: Luis.Serrano@uv.es

tion (DFT/MRCI) approach [14] and the ab initio CASSCF/MRCI method [15,16]. It has been clearly shown that only the full account of the electronic correlation energy can provide results accurate enough to understand the chemical problem, and therefore the use of expensive QM methods and the corresponding limitation in the affordable molecular-size systems can be understood. Most of the experimental results to be rationalized have been, however, obtained in solvated—aqueous in general—environments, or correspond to measurements of oligonucleotide or DNA strands in different media. Thus, there is a clear necessity to include the effects of the environment and see how it modifies the accurate QM results obtained for the isolated system, which can, on the other hand, be safely compared with data in gas phase or molecular beams.

The most comprehensive theoretical procedures to deal with the effects of the surrounding environment in chemical processes involve the coupling of the QM molecular core with a modeling of the external effects by means of molecular mechanics (MM) procedures that take into account dielectric, electrostatic, and steric interactions as well as the dynamic aspects of the problem. In order to tackle the issue of large systems at a reasonably computational cost, QM/MM methods represent, perhaps, one of the best alternatives. However, it has to be clear that these hybrid methods work because of error cancellations that are able to minimize the unbalanced description performed in the frontier region as well as in the non-symmetrical evaluation of the interactions in the QM and MM regions. Since their initial formulations [17], the QM/MM procedures in their many derivations (see, e.g., some recent reviews in refs. [18,19]) have been largely developed to treat many different chemical problems in organic chemistry, liquid-phase organic and organometallic chemistry, biochemistry, solid-state chemistry, and, only recently, photobiology (see, e.g., [20]). In the specific case of the DNA, QM/MM studies have been carried out mainly to analyze enzymatic, reactivity, or charge-transfer (CT) processes in the ground state (see, e.g., [21–24]), and few to study excited-state phenomena [25], whereas, as far as we know, the present one is the first report in which the employed QM approach fully includes on the excited state the electronic correlation energy (necessary to obtain quantitative answers) through the CASPT2 approach [26–29]. Our present goal is to illustrate, with a survey of examples, the capability of the approach to provide answers in the field of DNA properties, reactivity, and, especially, photoreactivity. Many of the examples shown here are parts of a more comprehensive ongoing study that is currently being developed on the DNA photoreactivity addressed to complement our previous studies on the isolated systems [30]. In particular, we will first discuss the oxidative and reductive capabilities of the NABs by analyzing their IPs and EAs, from the monomer to the nucleoside and nucleotide, focusing on cytosine, studying its IPs and EAs in isolation and embedded in a DNA strand, which will be modeled with the QM/MM methodology. Secondly, the use of QM/MM as a tool to provide proper structural constraints shall be analyzed for geometry optimization problems by studying the photoreversibility of the cyclobutane cytosine (CBC) dimer (C<>C) as an isolated dimer and that confined in a DNA strand. Finally, the emissive and nonadiabatic relaxation processes of a DNA analogous, 2-aminopurine, in the gas phase and solution will be discussed in the context of a solvation model. Unless indicated, all reported calculations used the MOLCAS QM package [31,32]. In the case of the QM/MM calculations, MOLCAS is linked to a modified version of the Tinker MM package [33].

METHODOLOGY

The QM/MM scheme employs as QM core the ab initio CASPT2//CASSCF multiconfigurational approach, a method that has repeatedly proved its accuracy in all types of electronic structure calculations and that is especially well suited to compute excited states [26–30,34–39]. The CASSCF level of theory was employed for the geometry optimizations, and dynamic electron correlation was taken into account perturbatively at the second-order level through the CASPT2 method. One-electron basis sets of atomic natural orbital (ANO) type ANO-S C,N,O[3s2p1d]/H[2s1p] (dimers) and ANO-L

C,N,O[4s3p1d]/H[2s1p] (monomers) were used throughout [31,32]. More specific details of the QM methodology, such as active spaces, will be mentioned when required.

The employed QM/MM strategy is based on an standard electrostatic embedding approach [40], using a hydrogen link atom scheme [41] to describe the frontier region placed at the glycosidic bond of the nucleoside (see Fig. 1). The MM subsystem has been represented using the AMBER99 forcefield [42]. Both subsystems (QM and MM) interact in the following way: (a) the QM wave function is polarized by all the MM point charges, (b) stretching, bending, and torsion potentials involving at least one MM atom are described at the MM level, and (c) standard van der Waals potentials are used to represent the interaction between atom pairs (QM-MM) separated by more than two bonds. Therefore, the Hamiltonian used in the computations takes the following form:

$$\hat{H} = \hat{H}_{\mathrm{QM}} + \hat{H}_{\mathrm{MM}} - \sum_{i=1}^{n}\sum_{j=1}^{Q}\frac{q_j}{r_{ij}} + \sum_{i=1}^{N}\sum_{j=1}^{Q}\frac{Z_i q_j}{R_{ij}} + E_{\mathrm{vdW}} + E_{\mathrm{frontier}} \tag{1}$$

where $\hat{H}_{\mathrm{QM}}$ is the Hamiltonian of the QM subsystem in vacuo, $\hat{H}_{\mathrm{MM}}$ is the Hamiltonian of the MM subsystem computed using the AMBER force field, and the remaining four terms are the interacting QM/MM Hamiltonian, with the first two terms comprising the electrostatic interactions (polarization of the wavefunction by the MM charges and Coulomb term between QM and MM nuclei, that in the optimizations carried out have been approximated using the electrostatic potential fitted (ESPF) operator method [43]), the third one corresponding to the van der Waals (vdW) interaction term computed using the definition of the AMBER force field, and the last one containing the terms needed for a proper description of the frontier within the hydrogen link-atom scheme. Within this model, the MM charges remain constant through the computation, and no polarization of the MM region is taken into account with an explicit term (yet polarization is included in a mean-field way in the parametrization of the AMBER point charges [42]). During the optimizations, the MM region surrounding the QM subsystem within

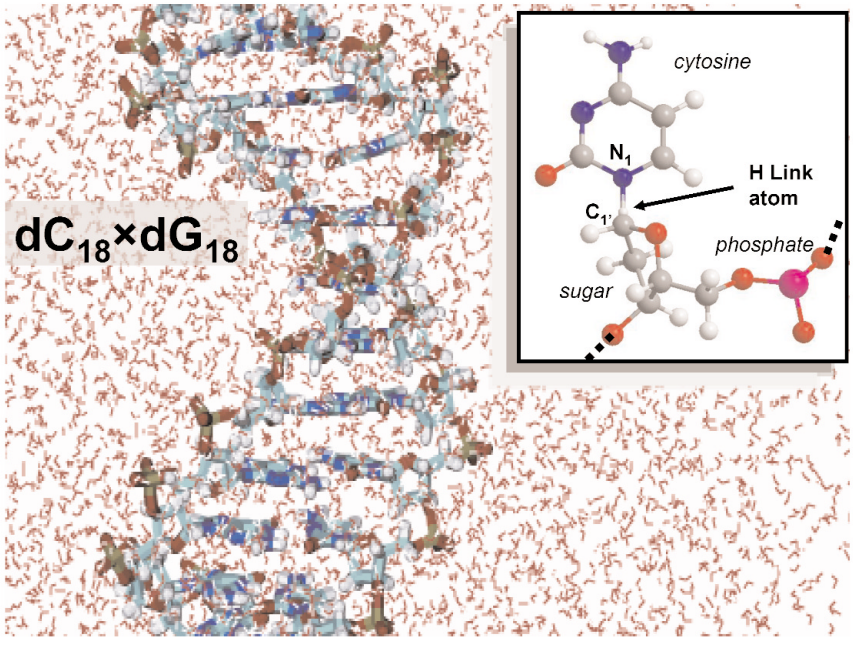

Fig. 1 An 18-base-pair long double helix of poly(C)-poly(G) ($dC_{18} \times dG_{18}$) surrounded by water molecules and the definition of the hydrogen link atom in the *N*-glycosidic bond between the N_1 of cytosine and $C_{1'}$ of sugar cycle.

5 Å has been allowed to relax using the microiterations technique (see, e.g., [44]). Examples of successful QM/MM applications on fast chemical processes in biological compounds can be found in the literature [45–47]. All the new computations reported here have been carried out using version 7.3 of the MOLCAS package [31,32,48].

RESULTS AND DISCUSSION

Ionization potentials and electron affinities of cytosine in DNA

The electron donor and acceptor abilities of the DNA and RNA subsystems such as NABs, nucleosides, nucleotides, or a pair of stacked bases are crucial to understand a great amount of phenomena related to DNA (see, e.g., [3–6,30,49–51]). Recently, we applied high-level QM ab initio coupled-cluster (CC) and multiconfigurational perturbation theory methods (CASPT2) [26,52] to compute the vertical and adiabatic ionization potentials (VIPs and AIPs, respectively) and electron affinities (VEAs and AEAs, respectively) of the canonical RNA and DNA bases, uracil, thymine, cytosine, adenine, and guanine in vacuo, establishing theoretical reference values for these properties at a level of theory not reported before [3,4]. The sequence of VIPs was found to be U > T > C > A > G covering the range of energies 9.42–8.09 eV, with uracil and guanine being the least and most favorable, respectively, for electron withdrawal, a trend that is maintained for the adiabatic property with a decrease in the energetic domain down to 9.12–7.65. The values are just in the experimental range for the vertical values and slightly lower for the adiabatic ones. In the case of VEAs (a poorly known property), the opposite trends as for IPs are obtained: guanine appears to be the least favorable to electron attachment (–1.14 eV), followed by adenine (–0.91 eV), cytosine (–0.69 eV), uracil (–0.61 eV), and thymine (–0.60 eV). As a consequence of the geometry relaxation of the charged systems that is taken into account in the adiabatic properties, the AEAs become closer to positive energy values. Adenine becomes the NAB with the most negative AEA, –0.57 eV, followed by guanine, whose energy increases to –0.35 eV, whereas cytosine, thymine, and uracil become very close to zero. In order to determine the role of the sugar and phosphate moieties and the source of the lowest IP in nucleosides and nucleotides, the lowest VIPs of 2'-deoxythimidine 5'-monophosphate (dTMP–) and 2'-deoxyguanidine 5'-monophosphate (dGMP–) were determined at the CASPT2//MP2 level of theory [49,53]. In all cases, and independently of the conformation, the lowest ionization channel is found related to a π-orbital of the NAB, an established concept [54] that had been wrongly questioned on the basis of DFT calculations [55]. The effect of adding a sugar group to the isolated NAB makes the VIP decrease in the thymine nucleoside by near 1 eV, whereas a further 3 eV lowering is observed (down to 6.0 eV) in the nucleotide as the negatively charged phosphate moiety is incorporated.

In a step toward the understanding of DNA behavior in the common cellular conditions under oxidative and reductive stress, it is of great importance to consider the effect of the medium surrounding the subsystems previously studied in vacuo. Therefore, we have carried out computations of the VIP, AIP, VEA, and AEA of NABs, starting with cytosine, applying a QM/MM approach to a system of one cytosine molecule embedded in a 18-base-pair long double helix of poly(C)-poly(G) (hereafter $dC_{18} \times dG_{18}$) surrounded by water molecules (see Fig. 1). In this initial model (to be followed by more extensive calculations), the sugar and phosphate moieties are treated at the MM level and we focus only on the IPs related with the NAB. Table 1 compiles the six low-lying IPs of cytosine in vacuo and in $dC_{18} \times dG_{18}$. The same level of theory, CASPT2(IPEA = 0.25)/ANO-L 431/21//CASSCF/ANO-L 431/21, is employed for the QM calculations in both cases [3,52]. The active space comprises all the π system plus the two in-plane oxygen and nitrogen lone-pair orbitals, conforming a space of 14 electrons distributed in 10 orbitals (14/10). The character of the related state of the cation is described by the type of molecular orbital (MO) where the unpaired electron is essentially placed. All the computed cation states are higher in energy at the molecule ground-state geometry when the double strand and the aqueous media are taken into account, except the π_2-state which becomes the cation state with the lowest VIP

in the QM/MM calculation. The difference between the lowest-lying VIP in vacuo and in the medium is therefore 0.66 eV, being less favorable to detach an electron from a cytosine molecule in the hydrated poly(C)-poly(G) double strand. Unlike what occurred in the isolated nucleoside and nucleotide, the IPs of embedded NABs do not decrease so dramatically as compared to the isolated values. One of the reasons is the balance imposed by the counterions that approach the negatively charged phosphate group. The states related with the oxygen and nitrogen lone-pair MOs undergo the largest increases in energy, especially that of the oxygen which becomes in the $dC_{18} \times dG_{18}$ model higher in energy than the n_N-state (cf. Table 1). Since these lone pairs are implied in the H-bonds between cytosine and its complementary NAB (guanine) in the double helix, their electron density around the nitrogen and oxygen atoms is lower and the electron detachment from their lone pairs is less favorable.

Table 1 Computed VIPs (in eV) of cytosine in vacuo and embedded in a double helix of hydrated $dC_{18} \times dG_{18}$.

State	In vacuo[a]	DNA
π_1	8.73	9.66
π_2	9.49	9.39
π_3	11.84	12.35
$\pi\,NH_2$	12.71	13.13
n_O	9.42	10.83
n_N	9.88	10.79

[a]Refs. [3,49].

Table 2 compiles the low-lying vertical and adiabatic IPs and EAs of cytosine in vacuo and inside $dC_{18} \times dG_{18}$. As in the case of the VIPs, the CASPT2(IPEA=0.25)//CASSCF/ANO-L 431/21 methodology has been employed for the QM calculations of AIPs, VEAs, and AEAs. When the DNA and the water environment are taken into account, all NAB VIPs have been found larger than for the isolated case. Additionally, the lowest VIP in the neutral embedded molecule at 9.39 eV corresponds to the π_2 orbital, that is, the HOMO-1 of the isolated system. When relaxing the geometry of the embedded system the π_1 (HOMO in the isolated cytosine) state of the cation becomes more stable, and therefore the AIP, 8.35 eV, is 0.26 eV lower than the value in vacuo, with a structure inside the DNA in which the amino group leaves the planarity displayed in vacuo. In the case of the VEAs, the presence of the environment increases the value 0.35 eV, still being negative. The geometrical relaxation increases the gas-phase EA by 0.65 eV from the vertical value, but it has even much more dramatic consequences for cytosine in DNA, making the attachment of an electron finally favorable in the biological environment. The AEA becomes positive, 0.69 eV, whereas the molecule acquires a nearly planar arrangement, in contrast to the ring distortion computed in vacuo.

As mentioned above, the present study will be complemented by computing all the NABs and enlarging the fragment included in the QM part. The CASPT2 method was also employed with systems of two adjacent cytosine–cytosine and adenine–cytosine NABs in a face-to-face conformation or in the B-form of DNA to compute the VIP and the VEA [50,51]. As a consequence of the stacking interactions between the NABs, stabilizations between 0.3 and 0.6 eV occur in the cationic and anionic systems. All these effects affect the acceptor and donor capabilities of the different subsystems of DNA and therefore represent the intrinsic abilities of these molecules in the process of electron attachment or detachment, having important consequences in the description of phenomena as CT along the DNA strand or in-site mutations [2,5,6,50]. Continuous efforts to provide accurate theoretical values with reliable methods such as CASPT2 and proper environment representation are required in the field.

Table 2 Computed lowest vertical and adiabatic IPs and EAs (in eV) of cytosine in vacuo and embedded in $dC_{18} \times dG_{18}$.

	In vacuo	DNA
VIP	8.73[a]	9.39[c]
AIP	8.61[b]	8.35[c]
VEA	–0.91[b]	–0.56
AEA	–0.26[b]	0.69

[a]Refs. [3,49].
[b]CASPT2(IPEA=0.25)/ANO-L 431/21//CASSCF/ANO-L 431/21. See also refs. [3,4].
[c]VIP from π_2 and AIP from π_1.

Photoreversibility of cyclobutane cytosine (CBC) dimer: A QM/MM approach

Cyclobutane pyrimidine dimers (Pyr<>Pyr or CPDs) formed by adjacent pyrimidine bases were the first discovered environmentally induced DNA lesions [56,57], and they can be considered the most frequent adducts photoinduced in UV-irradiated cellular DNA [58,59]. Understanding the mechanism of Pyr<>Pyr production and reversibility could help to propose ways of protection of the cell against the photodamage or strategies to repair the photolesion and restore the pyrimidines to their native state, parallel to the mechanism of DNA-photolyase enzymatic repair. Recently, we have analyzed the molecular basis of the photoproduction of CBC dimer (C<>C or CBC) along the singlet and triplet manifold, proving the crucial role of excited stacked dimers (excimers) as precursors of the photolesion [8]. Whereas a singlet–triplet crossing $(T_1/S_0)_X$ mediates the nonradiative deactivation toward the CBC dimer along a barrierless profile, the excimer has a highly stacked and bound face-to-face conformation in the singlet manifold such as the system has to overcome a barrier of 0.2 eV to reach the CI between the ground (S_0) and lowest singlet excited (S_1) states, $(S_1/S_0)_{CI}$, which connects the excimer and photoproduct. We have also explained the relationship between the efficiency of the production of the CBC dimer and the orientation of the pyrimidines at the time of irradiation with the relative position between the $(S_1/S_0)_{CI}$ crossing and the excimers formed by the adjacent stacked NABs. Therefore, reactive orientations are those that at the time of light irradiation are close but energetically above the CI, and the yield of formation of each conformation will strongly depend on the dynamics of the DNA strand, whose flexibility allows for long-range nuclear motions. It is interesting to compare the reaction intermediate formed in the triplet manifold, in which only one C_6–$C_{6'}$ intermonomer covalent bond is formed while C_5–$C_{5'}$ remains separated 2.8 Å (C_5 and C_6 are the double C=C bond atoms in cytosine), with that in the singlet manifold, in which the intermediate complex at the CI have intermonomer C–C distances close to 2.2–2.3 Å. The singlet manifold intermediate undoubtedly requires a better stacked and restrained structure of the two monomers than in the case of the triplet manifold intermediate. This can be an explanation of the suggested predominance of the triplet mechanism in solution, where diffusion (and spin-orbit coupling) would basically control the photoreaction, whereas the singlet mechanism is proposed to be more important in a constrained environment such as DNA [8,60]. In a subsequent study [61], we have compared the intrinsic production of the photodimer of cytosine (CBC) and thymine (CBT) in the singlet manifold and we have found that, in thymine, even the conformation of the two NABs with the largest binding energy is energetically above the CI, which explains the higher reactivity of thymine in the process of photodimerization. We also have suggested that irradiation of the photoproduct can lead to the cleavage of the C_5–$C_{5'}$ and C_6–$C_{6'}$ bonds of the Pyr<>Pyr reversing thus the photolesion. This reversibility is less favorable in the case of thymine since it requires more energy.

Up to now, our studies of the NAB dimers were focused on the intrinsic mechanism of photoproduction and photoreversibility of CBC and CBT dimers in vacuo. In order to determine the influence of the DNA environment on the photoreactivity of the dimers, we are currently carrying out calculations of the two pyrimidines embedded in the $dC_{18} \times dG_{18}$ double helix model employing QM/MM computational strategies. In the present report we would like simply to highlight one of the uses and advantages of the QM/MM methodology in the determination of molecular geometries and reaction paths, as well as to validate at this level the accuracy of the results obtained for the isolated system [8,61]. When determining the optimal geometry of the cytosine or thymine excimers in its lowest-excited singlet state we found out that, in order to prevent arrangements of the two monomers that could not possibly occur in DNA because of steric constraints, a designed practical solution was to work initially within the C_s symmetry. Such constraint was found preferable to other geometrical restrictions because it allowed explicitly the description of the conformations favorable for excimer and intermediate complexes formation. As an illustration we will show the connection between the low-lying S_1 singlet state of the CBC dimer and the face-to-face bound excimer conformation (C*C), a reaction path which represents the photoreversibility mechanism of the lesion. Figure 2 displays the low-lying singlet excited states of the isolated cytosine dimer computed at the CASPT2//CASSCF(12,12)/ANO-S 321/21 level along the minimum energy path (MEP) of the S_1 state from the CBC dimer at its ground-state equilibrium geometry. The active space comprises 12 π-orbitals except the two π-MOs localized in the NH_2 fragments and the plus and minus linear combinations of the deeper all-in-phase π-MOs of the two cytosine molecules. The S_1-MEP ends at the relaxed excimer ^{1}(C*C), and, close to MEP coordinate 4.5 au, shows a near-degenerate situation with the ground state which is closely related to the $(S_0/S_1)_{CI}$ CI structure. As the calculations are performed within the C_s symmetry, both states do not effectively cross, but the obtained structure is a good candidate as initial trial to search for a crossing at the CASPT2 level and with no symmetry restrictions, as it was performed in the previous study [8], despite the complexity of the calculations. For the sake of a more realistic description of the system, we introduced environmental effects through the QM/MM formalism, allowing also the pair of basis to move with no restrictions within the strands of the DNA model. We report in the present contribution the employment of the QM/MM methodology to study the photoreversibility of the CBC dimer using as a system the $dC_{18} \times$

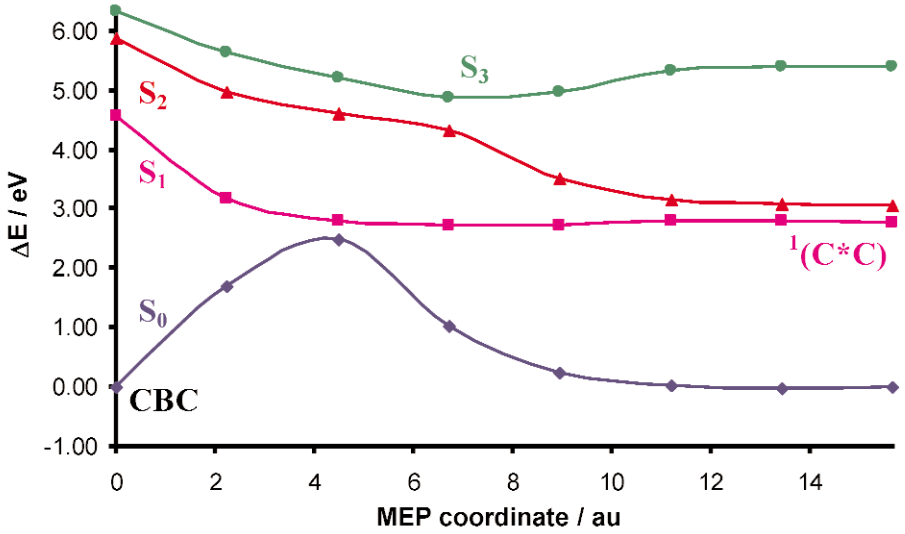

Fig. 2 Low-lying singlet excited states of the cytosine dimer computed at the CASPT2//CASSCF level along the MEP of the S_1 state from the CBC dimer at its ground-state equilibrium geometry. The S_1-MEP ends at the relaxed excimer ^{1}(C*C).

dG_{18} double helix presented above (see Fig. 1). Figure 3 displays the potential energy surfaces of the ground (S_0) and the lowest excited singlet (S_1) states of the cytosine dimer inside the chain $dC_{18} \times dG_{18}$ obtained along the geometry optimization process of the S_1 state of the CBC compound employing the QM/MM approach and the same ab initio level of theory. The starting structure corresponds to the ground-state equilibrium geometry of the CBC dimer where the adjacent cytosine molecules are linked through the C_5–$C_{5'}$ and C_6–$C_{6'}$ bonds. As in the case of the in vacuo CBC S_1-MEP, the energy difference between S_0 and S_1 along the optimization path decreases progressively, and reaches a region where both states are degenerate ($\Delta E < 0.2$ eV). As can be readily seen in Fig. 3, the geometry of the system at this point is of rhomboid type in accordance with the structure of the $(S_0/S_1)_{CI}$ CI in the final unconstrained CASPT2 results for the isolated system [8], something that the purely C_s optimization could not provide.

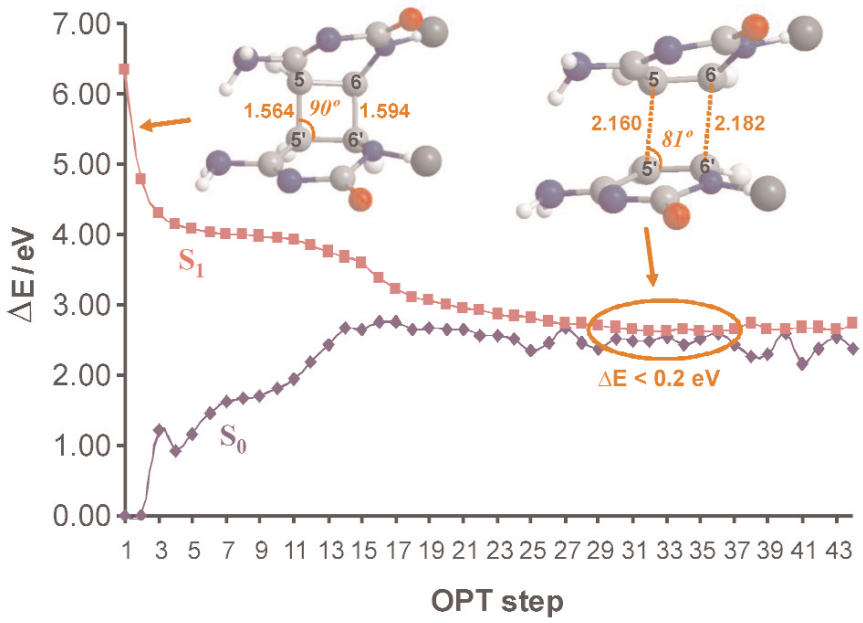

Fig. 3 Low-lying singlet excited states of the cytosine dimer inside the $dC_{18} \times dG_{18}$ double helix computed at the CASSCF level in the QM/MM approach along the optimization path of the S_1 state from the CBC dimer at its ground-state equilibrium geometry.

Emission and non-adiabatic decay of 2-aminopurine in the gas phase and water

2-Aminopurine is a constitutional isomer of adenine widely used as an emissive probe for monitoring DNA dynamics and conformational changes because, unlike adenine (6-aminopurine), it is highly fluorescent and minimally perturbs the DNA structure when substituting the natural NAB [62]. The modern description of the photochemistry of DNA NABs is based on recent works that explain the efficiency of radiationless decay between different electronic states by crossings of different potential energy hypersurfaces (PEHs), named conical intersections (CIs) (see, e.g., refs. [63,64]). These crossings behave as energy funnels where the probability for nonadiabatic, nonradiative jumps, that is, efficient internal conversion processes, is high [65,66]. Therefore, fluorescence quantum yields and excited lifetimes can be related to the nature of the paths and the barriers that the system has to surmount to reach the crossing seam. We recently explained the distinct photochemical behavior of the non-natural and highly emissive 2-aminopurine molecule and its weakly emissive natural isomer adenine in terms of

MEPs, reaction barriers, and accessibility of significant CIs [63,67]. Whereas adenine was shown to display a barrierless energy reaction path along its spectroscopic ππ* state toward an accessible CI connecting the excited and ground (gs) states, and enabling an efficient, ultrafast non-radiative decay, the equivalent path for 2-aminopurine contained an energy barrier hindering the access to the CI, and consequently increasing the excited state lifetime and leading to emission. The environment plays a significant role in the emissive properties of 2-aminopurine. For example, its fluorescence yield increases dramatically as the solvent polarity increases. For its close 9-ethyl-2-aminopurine derivative, the quantum yield varies from 0.01 in the nonpolar solvent cyclohexane to 0.68 in water [68]. In terms of PEHs the increase of the fluorescence yield should mean that the accessibility of the radiationless decay funnel (i.e., the CI) is more difficult in the polar environment, increasing the state lifetime and the probability of emission from the state minimum. It would be significant to perform calculations mimicking the effects of the solvent that could help to reinforce the photochemical paradigm based on the CI-accessibility concept [63,64].

In order to understand the distinct relaxation and emission properties of 2-aminopurine, we have used the sequential Monte Carlo quantum mechanics (S-MC/QM) approach in which the hydrated environment is modeled by the inclusion of different shells of 400 water molecules mimicked by a distribution of point charges. Statistically uncorrelated solute-solvent configurations are first generated for the subsequent quantum mechanics calculations [69–71]. As a strategy we have employed the different points belonging to the MEP computed at the CASPT2//CASSCF(16/13)/6-31G(d,p) level of theory for the isolated system in its initially populated ππ* (L_a) excited state [63], and at each of such geometries the solvation has been simulated as described. The QM calculations employed the MOLCAS package [31,32], whereas the MC simulations used the DICE program [72]. More technical details can be found elsewhere [73]. Our CASPT2 results in the gas phase indicate that the MEP leads the system along the lowest singlet excited ππ* state from the Franck–Condon region toward the minimum of the state, and further a barrier (computed as a transition state) of 2.4 kcal/mol has to be surmounted to reach the CI connecting with the ground state, $(gs/\pi\pi^*)_{CI}$ [63]. In solution, whereas the MEP toward the state minimum remains barrierless, the barrier required to reach the CI increases to 5.5 kcal/mol, representing an enhancement of 3.1 kcal/mol from the gas-phase situation. The CI, which remains as a degeneracy in solution, decreases its energy with respect to the minimum in the polar media by 7.4 kcal/mol, but this fact has no consequences for the photophysics of the system because the importance relies in the net increase of the energy barrier, which makes the access to the CI less probable [73]. Within this context, it is understandable that emission quantum yields measured near 0.02 in nonpolar solvents increase to 0.68 in water [68]. This result is particularly important because it helps to firmly establish the validity of the CI concept in photochemistry. Previous models such as the proximity effect scheme would have related the fluorescence quenching (here in the gas phase) with the coupling of ππ* and nπ* states that transfer the energy to hot levels of the ground state, whereas the strong emission in water would be attributed to the destabilization (and subsequent poorer coupling) of the nπ* state in the protonated environment [74]. As we showed previously [63], the nπ* state remains in a totally different region of the configuration space, far from where most of the energy evolves to, therefore, it can hardly be attributed any role in the emissive properties. In contrast, we show that they can be explained just by considering the fate of the bright spectroscopic ^1L_a ππ* state and the corresponding barriers to access the CI that leads to the decay to the ground state. This is consistent with the relative values of dipole moments. A slightly lower dipole moment of the transition state with respect to the minimum causes its relative destabilization in its interaction with the solvent, increasing the energy barrier [73].

ACKNOWLEDGMENTS

Financial support is acknowledged from projects CTQ2007-61260 and CSD2007-0010 Consolider-Ingenio in Molecular Nanoscience of the Spanish MEC/FEDER and GVPRE-2008-059 of the

Generalitat Valenciana. P.B.C. acknowledges a "Juan de la Cierva" contract from the Spanish MEC, and V.L. thanks the Universitat de València for financial support.

REFERENCES

1. C. E. Crespo-Hernández, B. Cohen, P. M. Hare, B. Kohler. *Chem. Rev.* **104**, 1977 (2004).
2. See, e.g., J. Leszczynski, M. Shukla (Eds.). *Radiation Induced Molecular Phenomena in Nucleic Acids. A Comprehensive Theoretical and Experimental Analysis*, Springer, New York (2008).
3. D. Roca-Sanjuán, M. Rubio, M. Merchán, L. Serrano-Andrés. *J. Chem. Phys.* **125**, 084302 (2006).
4. D. Roca-Sanjuán, M. Merchán, L. Serrano-Andrés, M. Rubio. *J. Chem. Phys*. **129**, 095104 (2008).
5. J. Leszczynski (Ed.). *Computacional Molecular Biology*, Elsevier, Amsterdam (1999).
6. L. A. Ericsson (Ed.). *Theoretical Biochemistry. Processes and Properties in Biological Systems*, Elsevier, Amsterdam (2001).
7. G. Olaso-González, D. Roca-Sanjuán, L. Serrano-Andrés, M. Merchán. *J. Chem. Phys.* **125**, 231102 (2006).
8. D. Roca-Sanjuán, G. Olaso-González, I. González-Ramírez, L. Serrano-Andrés, M. Merchán. *J. Am. Chem. Soc*. **130**, 10768 (2008).
9. J. J. Serrano-Pérez, M. Merchán, L. Serrano-Andrés. *J. Phys. Chem. B* **112**, 14002 (2008).
10. M. P. Fülscher, L. Serrano-Andrés, B. O. Roos. *J. Am. Chem. Soc.* **119**, 6168 (1997).
11. M. Merchán, L. Serrano-Andrés, M. A. Robb, L. Blancafort. *J. Am. Chem. Soc.* **127**, 1820 (2005).
12. S. Perun, A. L. Sobolewski, W. Domcke. *J. Phys. Chem. A* **110**, 13238 (2006).
13. H. Chen, S. H. Li. *J. Chem. Phys.* **124**, 154315 (2006).
14. C. M. Marian. *J. Phys. Chem. A* **111**, 1545 (2007).
15. K. A. Kistler, S. Matsika, *J. Phys. Chem. A* **111**, 2650 (2007).
16. M. Barbatti, H. Lischka. *J. Am. Chem. Soc*. **130**, 6831 (2008).
17. A. Warshel, M. Levitt. *J. Mol. Biol*. **103**, 227 (1976).
18. H. M. Senn, W. Thiel. "Atomistic approaches in modern biology: From quantum chemistry to molecular simulations", in *Topics in Current Chemistry*, Vol. 268, M. Reiher (Ed.), p. 173, Springer, Berlin (2007).
19. H. Lin, D. G. Truhlar. *Theor. Chem. Acc*. **117**, 185 (2007).
20. A. Sinicropi, T. Andruniow, L. De Vico, N. Ferre, M. Olivucci. *Pure Appl. Chem*. **77**, 977 (2005).
21. A. R. Dinner, G. M. Blackburn, M. Karplus. *Nature* **413**, 752 (2001).
22. P. Lin, V. K. Batra, L. C. Pedersen, W. A. Beard, S. H. Wilson, L. G. Pedersen. *Proc. Natl. Acad. Sci. USA* **105**, 5670 (2008).
23. F. Masson, T. Laino, I. Tavernelli, U. Rothlisberger, J. Hutter. *J. Am. Chem. Soc*. **130**, 3443 (2008).
24. T. Kubar, M. Elstner. *J. Phys. Chem. B* **112**, 8788 (2008).
25. G. Groenhof, L. V. Schäfer, M. Boggio-Pasqua, M. Goette, H. Grubmüller, M. A. Robb. *J. Am. Chem. Soc*. **129**, 6812 (2007).
26. K. Andersson, P.-Å. Malmqvist, B. O. Roos. *J. Chem. Phys.* **96**, 1218 (1992).
27. L. Serrano-Andrés, M. Merchán, I. Nebot-Gil, R. Lindh, B. O. Roos. *J. Chem. Phys*. **98**, 3151 (1993).
28. B. O. Roos, K. Andersson, M. P. Fülscher, P.-Å. Malmqvist, L. Serrano-Andrés, K. Pierloot, M. Merchán. *Adv. Chem. Phys.* **93**, 219 (1996).
29. M. Merchán, L. Serrano-Andrés. "Ab initio methods for excited states", in *Computational Photochemistry*, M. Olivucci (Ed.), Elsevier, Amsterdam (2005).

30. L. Serrano-Andrés, M. Merchán. "Photostability and photoreactivity", in *Biomolecules*: *Quantum Chemistry of Nucleic Acid Base Monomers and Dimers*, in *Radiation Induced Molecular Phenomena in Nucleic Acids. A Comprehensive Theoretical and Experimental Analysis*, J. Leszczynski, M. Shukla (Eds.), Springer, New York (2008).
31. G. Karlström, R. Lindh, P.-Å. Malmqvist, B. O. Roos, U. Ryde, V. Veryazov, P.-O. Widmark, M. Cossi, B. Schimmelpfennig, P. Neogrady, L. Seijo. *Comput. Mater. Sci.* **28**, 222 (2003).
32. V. Veryazov, P.-O. Widmark, L. Serrano-Andrés, R. Lindh, B. O. Roos. *Int. J. Quantum Chem.* **100**, 626 (2004).
33. TINKER, Software Tools for Molecular Design, version 4.2. J. W. Ponder, F. M. Richards. *J. Comp. Chem.* **8**, 1016 (1987).
34. L. Serrano-Andrés, M. P. Fülscher, B. O. Roos, M. Merchán. *J. Phys. Chem.* **100**, 6484 (1996).
35. J. Finley, P.-Å. Malmqvist, B. O. Roos, L. Serrano-Andrés. *Chem. Phys. Lett*. **288**, 299 (1998).
36. L. Serrano-Andrés, N. Forsberg, P.-Å. Malmqvist. *J. Chem. Phys*. **108**, 7202 (1998).
37. A. C. Borin, L. Serrano-Andrés. *Chem. Phys*. **262**, 253 (2000).
38. L. Serrano-Andrés, M. Merchán, R. Lindh. *J. Chem. Phys*. **122**, 104107 (2005).
39. M. Schreiber, M. R. Silva, S. P. A. Sauer, W. Thiel. *J. Chem. Phys*. **128**, 134110 (2008).
40. D. Bakowies, W. Thiel. *J. Phys. Chem.* **100**, 10580 (1996).
41. U. C. Singh, P. A. Kollman. *J. Comput. Chem.* **7**, 718 (1986).
42. J. P. Wang, P. Cieplack, P. A. Kollman. *J. Comput. Chem.* **21**, 1049 (2000).
43. N. Ferré, J. G. Ángyán. *Chem. Phys. Lett.* **356**, 331 (2002).
44. T. Vreven, K. Morokuma, Ö. Farkas, H. B. Schlegel, M. J. Frisch. *J. Comput. Chem*. **24**, 760 (2003).
45. P. B. Coto, A. Strambi, N. Ferré, M. Olivucci. *Proc. Natl. Acad. Sci. USA* **103**, 17154 (2006).
46. A. Strambi, P. B. Coto, L. M. Frutos, N. Ferré, M. Olivucci. *J. Am. Chem. Soc.* **130**, 3382 (2008).
47. P. B. Coto, S. Martí, M. Oliva, M. Olivucci, M. Merchán, J. Andrés. *J. Phys. Chem. B* **112**, 7153 (2008).
48. See MOLCAS webpage: <http://www.teokem.lu.se/molcas>.
49. M. Rubio, D. Roca-Sanjuán, M. Merchán, L. Serrano-Andrés. *J. Phys. Chem. B* **110**, 10234 (2006).
50. D. Roca-Sanjuán, M. Merchán, L. Serrano-Andrés. *Chem. Phys.* **349**, 188 (2008).
51. L. Serrano-Andrés, M. Merchán, D. Roca-Sanjuán, G. Olaso-González, M. Rubio. "Bioexcimers as precursors of charge transfer and reactivity in photobiology", in *Computational Methods in Science and Engineering. Theory and Computation: Old Problems and New Challenges*, T. Simos, G. Maroulis (Eds.), American Institute of Physics, Greece (2007).
52. G. Ghigo, B. O. Roos, P.-Å. Malmqvist. *Chem. Phys. Lett*. **396**, 142 (2004).
53. M. Rubio, D. Roca-Sanjuán, M. Merchán, L. Serrano-Andrés. *J. Phys. Chem. B* **113**, 2451 (2009).
54. M. Yan, D. Becker, S. Summerfield, P. Renke, M. D. Sevilla. *J. Phys. Chem.* **96**, 1983 (1992).
55. X. Yang, X.-B. Wang, E. R. Vorpagel, L.-S. Wang. *Proc. Natl. Acad. Sci. USA* **101**, 17588 (2004).
56. R. Beukers, J. Ijlstra, W. Berends. *Rec. Trav. Chim. Pays-Bas* **77**, 729 (1958).
57. R. Beukers, A. P. M. Eker, P. H. M. Lohman. *DNA Repair* **7**, 530 (2008).
58. J. Cadet, P. Vigny. In *Bioorganic Photochemistry*, H. Morrison (Ed.), John Wiley, New York (1990).
59. T. Douki, J. Cadet. *Biochemistry* **40**, 2495 (2001).
60. W. J. Schreier, T. E. Schrader, F. O. Soller, P. Gilch, C. E. Crespo-Hernández, V. N. Swaminathan, T. Carell, W. Zinth, B. Kohler. *Science* **315**, 625 (2007).
61. J. J. Serrano-Pérez, I. González-Ramírez, P. B. Coto, M. Merchán, L. Serrano-Andrés. *J. Phys. Chem. B* **112**, 14096 (2008).
62. E. L. Rachofsky, R. Osman, J. B. A. Ross. *Biochemistry* **40**, 946 (2001).
63. L. Serrano-Andrés, M. Merchán, A. C. Borin. *Proc. Natl. Acad. Sci. USA* **103**, 8691 (2006).
64. L. Serrano-Andrés, M. Merchán, A. C. Borin. *J. Am. Chem. Soc*. **108**, 2473 (2008).

65. M. Klessinger, J. Michl. *Excited States and Photochemistry of Organic Molecules*, VCH, New York (1995).
66. M. Olivucci (Ed.). *Computational Photochemistry*, Elsevier, Amsterdam (2005).
67. L. Serrano-Andrés, M. Merchán, A. C. Borin. *Chem.—Eur. J*. **12**, 6559 (2006).
68. D. C. Ward, E. Reich, L. Stryer. *J. Biol. Chem.* **244**, 1228 (1969).
69. S. Canuto, K. Coutinho. *Adv. Quantum Chem.* **28**, 89 (1997).
70. K. Coutinho, S. Canuto. *J. Chem. Phys*. **113**, 9132 (2000).
71. K. Coutinho, S. Canuto, M. C. Zerner. *J. Chem. Phys.* **112**, 9874 (2000).
72. K. Coutinho, S. Canuto. A Monte Carlo Program for Molecular Liquid Simulation. University of São Paulo, São Paulo, SP, Brazil (2000).
73. V. Ludwig, M. S. do Amaral, Z. M. da Costa, A. C. Borin, S. Canuto, L. Serrano-Andrés. *Chem. Phys. Lett*. **463**, 201 (2008).
74. E. C. Lim. *J. Phys. Chem.* **90**, 6770 (1986).